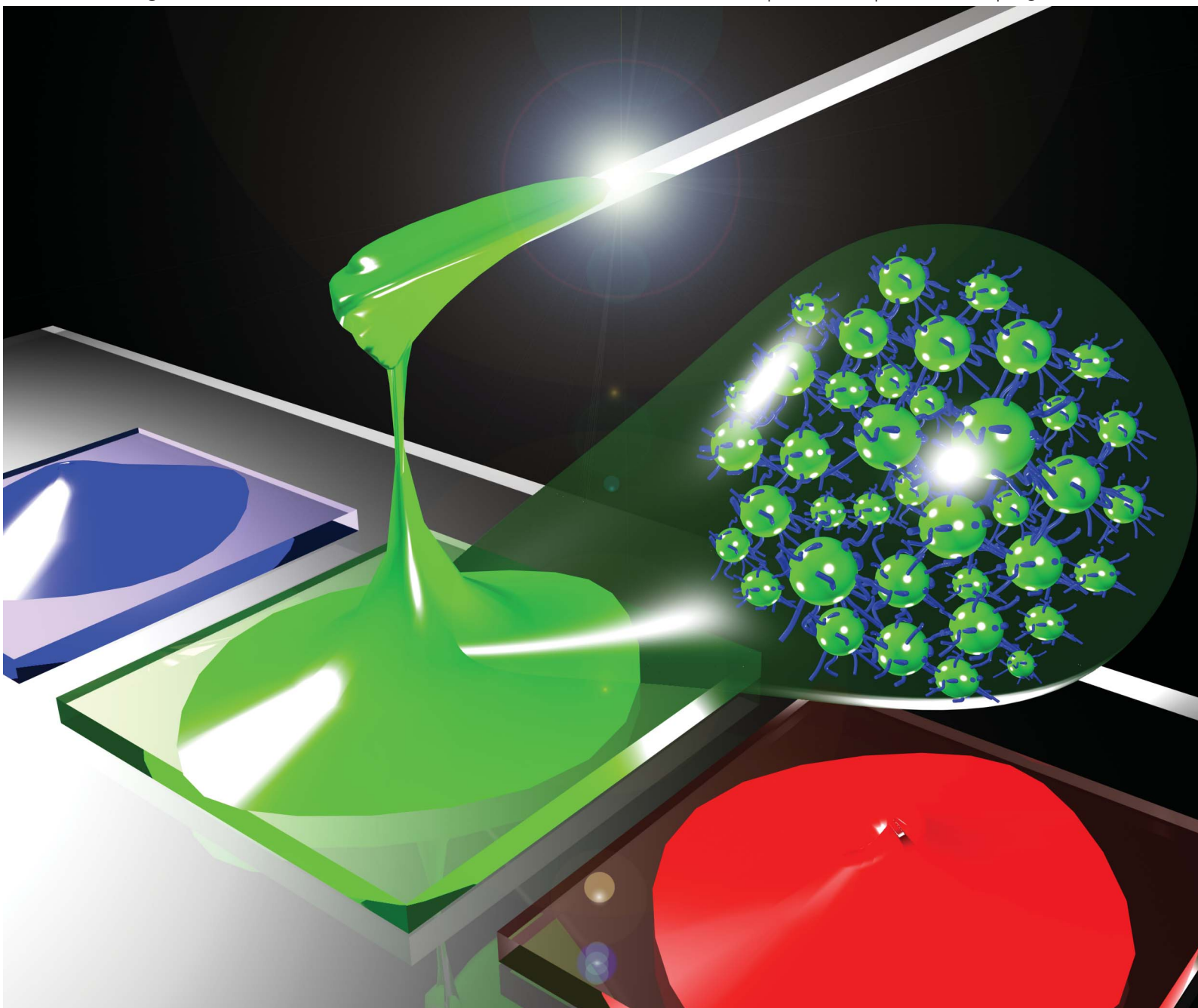


# Journal of Materials Chemistry

www.rsc.org/materials

Volume 22 | Number 23 | 21 June 2012 | Pages 11405–11862



ISSN 0959-9428

RSC Publishing

**PAPER**

Jinhan Cho *et al.*

Solvent-free nanoparticle fluids with highly collective functionalities for layer-by-layer assembly



0959-9428 (2012) 22:23;1-G

Cite this: *J. Mater. Chem.*, 2012, **22**, 11488

www.rsc.org/materials

PAPER

## Solvent-free nanoparticle fluids with highly collective functionalities for layer-by-layer assembly†

Younghoon Kim, Donghee Kim, Ilyoung Kwon, Hyun Wook Jung and Jinhan Cho\*

Received 10th February 2012, Accepted 13th March 2012

DOI: 10.1039/c2jm30815k

Here we demonstrate the successful preparation of solvent-free inorganic nanoparticle (NP) fluids with high functionalities that allow mass production. The inorganic NPs (Ag, Au, and quantum dots [QDs]) used in this study were directly synthesized using hydrophobic stabilizers such as palmitic acid, oleic acid, or tetraoctylammonium bromide in a nonpolar solvent (chloroform or toluene), and these NPs were directly phase-transferred to solvent-free low molecular weight liquid media (*i.e.*, thiol-containing imidazolium-type ionic liquid). The NP fluids formed at room temperature showed excellent functionalities (*i.e.*, long-term dispersion stability, high electrical conductivity, strong optical energy transfer, and high photoluminescent intensity) without requiring any additional process such as anion exchange or thermal processing. Furthermore, layer-by-layer deposition of QDs stabilized by the ionic liquid induced highly fluorescent properties compared to those of layer-by-layer QD multilayers prepared using conventional ligands such as mercaptoacetic acid or cysteamine, which mainly originated from the high packing density and the relatively high quantum efficiency of ionic liquid-stabilized QDs.

### Introduction

Solvent-free nanoparticle (NP) fluids<sup>1–4</sup> with liquid-like behavior at room temperature that are stabilized by ionic liquids (ILs)<sup>5–8</sup> in the absence of solvent media have recently attracted considerable attention due to the expected evolution of nanoscience and nanotechnology through the design of new functional nanomaterials with novel electronic, optical, and biological properties. These NP fluids have been mainly produced by the electrostatic grafting of a bulky organic layer onto the surface of charged NPs (*e.g.*, silica, iron oxide, and titania) to provide a fluidization medium. It was also reported that metal NP fluids could be prepared using polymer IL ligands *via* a five-step process including anion exchange.<sup>1–4</sup> The use of bulky organic ( $M_w > \sim 10^3$ ) or polymer IL ligands for the preparation of solvent-free NP fluids can provide the liquid-like behavior instead of solid form at room temperature. However, solvent-free NP fluids with bulky ionic groups have a limited ability to decrease the gap between neighboring NPs, which causes difficulty in the enhancing or controlling of collective functionalities (particularly electrical conductivity) among NPs within fluids. For example, most of the metal NP assembly processes reported by other research groups exhibited relatively high sheet

resistances  $>10^5 \Omega \square^{-1}$  at room temperature due to the particle-particle separation distances associated with the stabilizers having a bulky chain length.<sup>9–11</sup> As a result, metal NP assembly requires thermal annealing ( $>200^\circ\text{C}$ ) to obtain a sheet resistance  $<10^{-3} \Omega \square^{-1}$ . Furthermore, most of the inorganic NPs employed for NP fluids have been mainly synthesized in polar solvents (*i.e.*, water or alcohol).<sup>1,3,4</sup> It is well known that the quality (*i.e.*, uniform size, high crystallinity) and production efficiency of inorganic NPs synthesized in polar solvents are inferior to those of NPs synthesized in nonpolar solvent media such as toluene or hexane. Considering that inorganic NPs such as metals or quantum dots (QDs) have attracted significant attention in a variety of fields such as electronics and optics due to their size-dependent physicochemical properties,<sup>12</sup> it is critical to develop a general and facile approach to creating NP fluids with high functionality and quality as well as mass production ability.

Here we report on highly concentrated and uniform NP fluids with long-term dispersion stability, high electrical conductivity (for metal NP fluids), or strong optical tuning properties (for fluorescent QD NPs) at room temperature that allows for their mass production. In contrast to most IL ligands used for solvent-free NPs, which generally have bulky ion groups that are acquired *via* complex processes (*i.e.*, synthetic and ion exchange processes), the IL ligand used in our study has a short chain length and requires no additional ion exchange steps. For this investigation, Ag NPs ( $\text{Ag}_{\text{NPs}}$ ), Au NPs and QDs ( $\text{CdSe@ZnS}$ ) were first synthesized using hydrophobic stabilizers such as palmitic acid,<sup>13</sup> tetraoctylammonium bromide (TOABr),<sup>14</sup> and

Department of Chemical and Biological Engineering, Korea University, Anam-dong, Seongbuk-gu, Seoul 136-713, Korea. E-mail: jinhan71@korea.ac.kr; Fax: +82 2 926 6102; Tel: +82 2 3290 4852

† Electronic supplementary information (ESI) available. See DOI: 10.1039/c2jm30815k

oleic acid stabilizers<sup>15</sup> in a nonpolar solvent (*e.g.*, toluene or hexane), respectively, to achieve a uniform size dispersion, a high concentration, and mass production capabilities. After synthesis, NPs dispersed in toluene were directly phase-transferred to thiol-functionalized imidazolium-type IL (TFI-IL) media with a short chain length ( $M_w = 192.7 \text{ g mol}^{-1}$ ) and liquid behavior at room temperature. The TFI-IL- $\text{Ag}_{\text{NPs}}$  that were stabilized using short-chain ligands could be highly concentrated to >60 wt%, and a narrow gap between NPs caused a notably enhanced electrical conductivity ( $\sim 40 \text{ } \Omega \text{ } \square^{-1}$ ). This conductivity could be also decreased to  $< 10^{-3} \text{ } \Omega \text{ } \square^{-1}$  after thermal annealing at  $> 175 \text{ } ^\circ\text{C}$ . The TFI-IL-QDs exhibited significant optical energy transfer and high fluorescent intensity with relatively high quantum efficiency compared to those of conventional QDs dispersed in aqueous solution. To the best of our knowledge, electrical properties and optical tuning have not yet been considered in solvent-free NP fluids based on IL ligands. Furthermore, it has been demonstrated that TFI-IL-QDs dispersed in aqueous medium can be electrostatically assembled layer-by-layer (LbL)<sup>16–26</sup> with other negatively charged materials to achieve dense surface coverage (>45%) and high photoluminescence (PL) intensity due to the concentrated deposition solution and unique chemical properties of the TFI-IL ligands with cationic resonance structures. We believe that solvent-free NP fluids can be effectively applied to a variety of electronic/optical inks and films allowing desired functionalities without the need for additional synthetic processes or thermal treatment.

## Experimental section

### Materials

TFI-ILs were prepared as follows. 1-Methylimidazole (3.09 g, 37.67 mmol) and 3-chloro-1-propanethiol (5 g, 45.20 mmol) were refluxed for 72 h at  $80 \text{ } ^\circ\text{C}$  under argon-protected conditions.<sup>27,28</sup> PA- $\text{Ag}_{\text{NPs}}$ ,<sup>13</sup> TOABr- $\text{Au}_{\text{NPs}}$ ,<sup>14</sup> and OA-CdSe@ZnS<sup>15</sup> were synthesized as previously reported. These NPs dispersed in nonpolar solvent were phase-transferred to TFI-IL medium successively up to desired NP concentration.

### Build-up of multilayers

The concentration of the TFI-IL-QD deposition solution was controlled by the addition of water to solvent-free TFI-IL-QD at a concentration of 10 wt%. PSS were prepared at a concentration of  $1 \text{ mg mL}^{-1}$  by the addition of 0.2 M NaCl. Prior to LbL assembly, the quartz or silicon substrates were cleaned with RCA solution ( $\text{H}_2\text{O} : \text{NH}_3 : \text{H}_2\text{O}_2 : 5 : 1 : 1 \text{ v/v/v}$ ). The substrates were dipped into the TFI-IL-QD solution for 10 min and washed twice with DI water. The TFI-IL-QD-coated substrates were dipped into PSS dispersions for 10 min and washed with DI water. The resulting substrates were dipped into the TFI-IL-QD solution for 10 min. The above dipping cycles were repeated until the desired number of layers had been obtained.

### Measurements

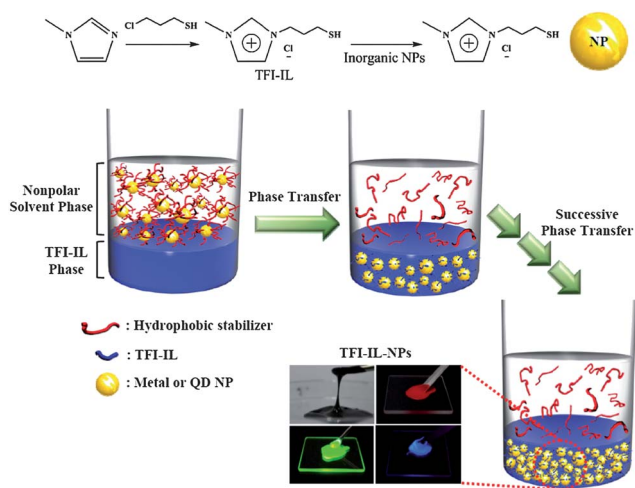
TFI-IL- $\text{Ag}_{\text{NP}}$  rheological properties, such as shear stress and shear viscosity, were measured using an MCR-301 (Anton Paar) rheometer at  $25 \text{ } ^\circ\text{C}$ . TFI-IL- $\text{Ag}_{\text{NP}}$  modulus data, including

elastic and viscous moduli, were obtained using the same rheometer *via* a temperature-sweep mode from  $25\text{--}80 \text{ } ^\circ\text{C}$  with a  $10 \text{ } ^\circ\text{C min}^{-1}$  rate under a fixed angular frequency ( $1 \text{ s}^{-1}$ ) and strain amplitude (10%). The electrical properties of TFI-IL- $\text{Ag}_{\text{NPs}}$  were measured using a four point probe station (Changmin Tech Co., Ltd., CMT-SR2000N). PL spectra were measured using fluorescence spectroscopy (Perkin Elmer LS 55). The PL spectra for (TFI-IL-QD/PSS) multilayers were measured at excitation wavelengths of  $\lambda_{\text{ex}} \approx 300 \text{ nm}$ . A QCM device (QCM200, SRS) was used to examine the mass of the material deposited after each adsorption step. The resonance frequency of the QCM electrodes was approximately 5 MHz. The adsorbed mass of TFI-IL-QD and PSS,  $\Delta m$ , was calculated from the change in QCM frequency,  $\Delta F$ , using the Sauerbrey equation:<sup>27</sup>  $\Delta F \text{ (Hz)} = -56.6 \times \Delta m_{\text{A}}$ , where  $\Delta m_{\text{A}}$  is the mass change per quartz crystal unit area in  $\mu\text{g cm}^{-2}$ . Although it was reported by Kasemo and co-workers that the Sauerbrey equation between adsorbed mass and frequency change has much difficulty in being applied to the viscoelastic, thicker or hydrogel layers containing water molecules in a solid-liquid interface,<sup>28–30</sup> the QCM measurements in our study were made after sufficiently drying the adsorbed layer using nitrogen gas. Additionally, the frequency changes contributed by PSS were measured to be below 3% compared to those of inorganic nanoparticles (*i.e.*, TFI-IL-QD), and furthermore the thickness of PSS is below 1.5 nm per layer. Therefore, PSS/TFI-IL-QD multilayers adsorbed onto the crystal surface can be regarded as rigid, evenly distributed, and sufficiently thin films satisfying the Sauerbrey equation.

## Results and discussion

The TFI-ILs used in our study were synthesized from 1-methylimidazole and 3-chloro-1-propanethiol.<sup>31,32</sup> The degradation temperature ( $T_d$ ) of TFI-IL was approximately  $175 \text{ } ^\circ\text{C}$ . Additionally, the viscous modulus,  $G''$ , was much higher than the elastic modulus,  $G'$ , over the measured temperature range, suggesting a liquid-like behavior (see ESI, Fig. S1†).<sup>33</sup> This TFI-IL can be used as a ligand-exchanging stabilizer for the phase transfer of various inorganic NPs (*e.g.*, Ag, Au, Pt, Pd, or QDs) from nonpolar solvents to the TFI-IL media due to the high affinity between the surface of NPs and thiol group of the TFI-IL (Scheme 1). In contrast, imidazolium-type ILs containing amine groups instead of thiol moieties do not induce a phase transfer for inorganic NPs dispersed in toluene. In addition, the imidazolium-type ILs containing amine groups only exhibit liquid behavior at temperatures  $> 60 \text{ } ^\circ\text{C}$  and are thus unusable as ink pastes at room temperature.

First, the palmitic acid- $\text{Ag}_{\text{NP}}$  (PA- $\text{Ag}_{\text{NP}}$ )  $\sim 8 \text{ nm}$  in size dispersed in toluene was exchanged with a TFI-IL ligand, increasing the transferred amount of  $\text{Ag}_{\text{NP}}$  to  $\geq 63 \text{ wt}\%$  (Fig. 1a). This approach can be applied to other metal NPs stabilized by a hydrocarbon stabilizer such as TOABr- $\text{Au}_{\text{NPs}}$  (see ESI, Fig. S2†). The  $\text{Ag}_{\text{NP}}$  contents in the TFI-IL- $\text{Ag}_{\text{NP}}$  fluids were obtained using thermogravimetric analysis (TGA) (ESI, Fig. S3†). It should be noted that the  $G''$  value of these samples was still greater than the  $G'$  value in the measured temperature range (*i.e.*,  $25\text{--}80 \text{ } ^\circ\text{C}$ ) (see ESI, Fig. S4†). As shown in Fig. 1b, the shear viscosity of TFI-IL- $\text{Ag}_{\text{NP}}$  increased with the  $\text{Ag}_{\text{NP}}$  content



**Scheme 1** Schematics for the preparation of TFI-IL and solvent-free inorganic nanoparticles stabilized by TFI-ILs.

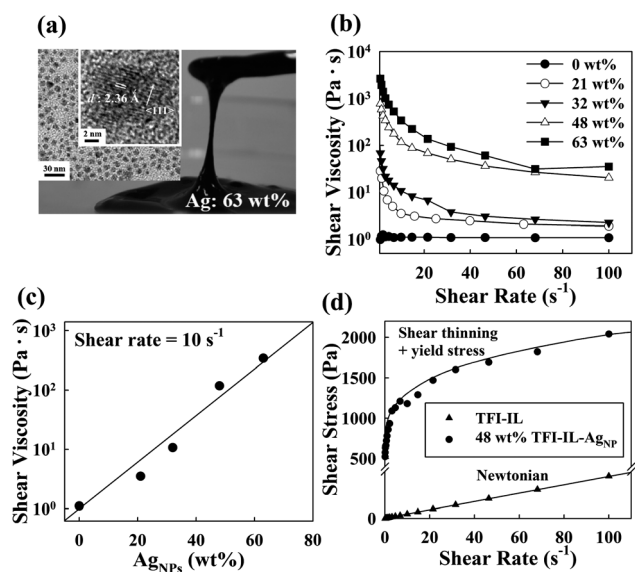


**Fig. 1** (a) Photographic image of the highly concentrated TFI-IL- $\text{Ag}_{\text{NP}}$  (63 wt%). The inset of (a) displays the TEM image of TFI-IL- $\text{Ag}_{\text{NP}}$ . (b) Shear viscosity data of TFI-IL- $\text{Ag}_{\text{NP}}$  as a function of shear rate. (c) Shear viscosity of TFI-IL- $\text{Ag}_{\text{NP}}$  measured at a shear rate of  $10 \text{ s}^{-1}$ . (d) Shear stress curves of TFI-IL and 48 wt% TFI-IL- $\text{Ag}_{\text{NP}}$  as a function of shear rate.

as a function of the shear rate. At a  $10 \text{ s}^{-1}$  shear rate, the shear viscosity of TFI-IL- $\text{Ag}_{\text{NP}}$  is proportional to the  $\text{Ag}_{\text{NPs}}$  content (Fig. 1c). Fig. 1d shows that the shear stress of TFI-IL increases linearly as a function of the shear rate, exhibiting rheological Newtonian behavior. In contrast, the shear stress of 48 wt% TFI-IL- $\text{Ag}_{\text{NP}}$  initially evolved from yield stress, requiring a certain stress to initiate the flow in the case of a low shear rate. These phenomena indicate that TFI-IL- $\text{Ag}_{\text{NP}}$  displays novel shear thinning behavior with yield stress, a non-Newtonian characteristic.<sup>34</sup>

Based on the fluidic behavior of TFI-IL- $\text{Ag}_{\text{NPs}}$ , we investigated electrical properties of TFI-IL- $\text{Ag}_{\text{NPs}}$  fluid. Fig. 2 shows

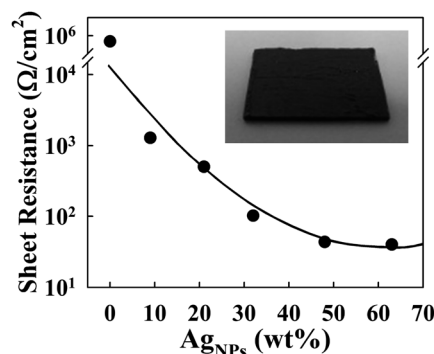


**Fig. 2** The sheet resistance of TFI-IL- $\text{Ag}_{\text{NP}}$  films prepared using the doctor blade method. The inset shows the TFI-IL- $\text{Ag}_{\text{NP}}$  film containing  $\text{Ag}_{\text{NPs}}$  of 63 wt%.

the sheet resistance of TFI-IL- $\text{Ag}_{\text{NPs}}$  as a function of  $\text{Ag}_{\text{NP}}$  quantity. The sheet resistances of 0, 9, 21, and 32 wt% TFI-IL- $\text{Ag}_{\text{NPs}}$  were  $6 \times 10^5$ , 1288, 501, and  $101 \text{ } \Omega \text{ } \square^{-1}$ , respectively. However, the sheet resistance approached a saturation value of  $40 \text{ } \Omega \text{ } \square^{-1}$  in the 48 wt% TFI-IL- $\text{Ag}_{\text{NPs}}$  sample that had not been thermally treated. The saturated sheet resistance implies that the minimum interparticle distance between  $\text{Ag}_{\text{NPs}}$  with liquid-like behavior (formed by the short-chain TFI-IL) was formed at 48 wt% TFI-IL- $\text{Ag}_{\text{NPs}}$ . Both tunneling (by distance between stabilizers) and close contact between  $\text{Ag}_{\text{NPs}}$  enable electron flow in the  $\text{Ag}_{\text{NP}}$  films.<sup>35,36</sup> In the case of using TOABr- $\text{Au}_{\text{NP}}$  instead of PA- $\text{Ag}_{\text{NP}}$ , the electrical phenomena of TFI-IL- $\text{Au}_{\text{NP}}$  fluid were very similar to those of TFI-IL- $\text{Ag}_{\text{NP}}$  fluid. In contrast, in the case of  $\text{Ag}_{\text{NPs}}$  which were stabilized by oleic acid, palmitic acid, and polymer, the films displayed a high sheet resistance of  $>10^5 \text{ } \Omega \text{ } \square^{-1}$  due to increased particle-particle separation distances associated with stabilizers with long chain length. Therefore, most of the  $\text{Ag}_{\text{NP}}$  assembly processes reported by other research groups require thermal annealing ( $>250 \text{ } ^\circ\text{C}$ ), possibly to decompose their stabilizers to obtain a low sheet resistance.<sup>9,37</sup> From this perspective, it should be noted that TFI-IL- $\text{Ag}_{\text{NP}}$  fluids are very effective for enhancing conductivity at room temperature because the short chain length of TFI-ILs enables shorter particle-particle distances and denser  $\text{Ag}_{\text{NPs}}$  networks compared to stabilizers with long chain lengths and high  $M_w$  values. In the case of TFI-IL- $\text{Ag}_{\text{NP}}$  fluids with thermal treatment  $>175 \text{ } ^\circ\text{C}$  ( $T_d$  of TFI-IL,  $\sim 175 \text{ } ^\circ\text{C}$ ), their sheet resistance was  $<10^{-3} \text{ } \Omega \text{ } \square^{-1}$ .

Furthermore, the reduced inter-particle distance induced by the TFI-IL stabilizers has a significant effect on the optical and electrical properties of NP assembly. To investigate these properties, approximately 48 wt% TFI-IL-QDs (*i.e.*, CdSe@ZnS) with liquid-like behavior were prepared using oleic acid (OA)-CdSe@ZnS with red ( $\lambda_{\text{max}} \approx 614 \text{ nm}$  for PL maximum peak and QD diameter ( $D$ )  $\approx 5.4 \text{ nm}$ ), green ( $\lambda_{\text{max}} \approx 528 \text{ nm}$  and  $D \approx 5.0 \text{ nm}$ ) and blue emissions ( $\lambda_{\text{max}} \approx 461 \text{ nm}$  for PL maximum peak and  $D \approx 4.5 \text{ nm}$ ) using ligand exchange (Fig. 3; ESI, Fig. S5†). In addition, TFI-IL-QD samples prepared by varying the loading amount of QDs showed the non-Newtonian behavior like the results of TFI-IL- $\text{Ag}_{\text{NPs}}$  (ESI, Fig. S6†). We found that the PL spectra of TFI-IL-QDs with strong PL intensity were dramatically red-shifted relative to those of OA-QDs despite

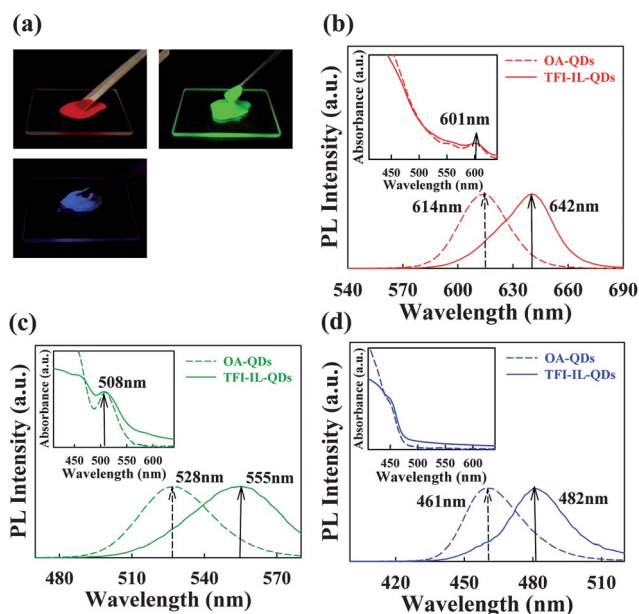


**Fig. 3** (a) Photo images of TFI-IL-QDs with liquid-like behavior prepared from red, green and blue emitting QDs after UV irradiation. Comparison of optical properties between OA-QDs and TFI-IL-QDs by UV-vis and PL spectroscopy of (b) red-QDs, (c) green-QDs and (d) blue-QDs, respectively.

having the same peak maxima in the UV-vis absorption spectra (Fig. 3b–d). This notable red-shift of the PL peaks results from an exciton energy transfer by dipole–dipole interactions among the closely packed QDs.<sup>38</sup> In addition, it was found that the more concentrated samples than 48 wt% TFI-IL-QD could not be prepared because OA-QDs dispersed in toluene were not phase-transferred to TFI-IL media any more. Therefore, it is reasonable to conclude that the concentration of TFI-IL-QDs and the red-shift of their PL were almost saturated at about 48 wt%. This finding supports our hypothesis that TFI-IL ligands effectively reduce the inter-particle distance between NPs, thereby enabling liquid-like behavior at room temperature. Furthermore, these results are very significant in that optical properties can be easily controlled by the QD loading amount within the fluids (Fig. 4).

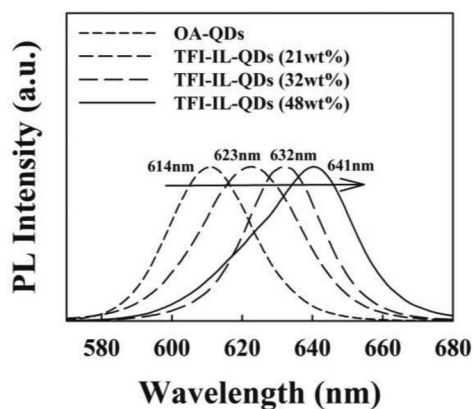


**Fig. 4** Change in PL spectra of TFI-IL-QD<sub>red</sub> with increasing the loading amount of TFI-IL-QD<sub>red</sub>.

Another advantage of TFI-IL-NPs is that with the use of cationic imidazolium, these NPs can be electrostatically assembled LbL using anionic materials such as poly(sodium, 4-styrenesulfonate) (PSS) in a wide range of different concentrations if water solvent is added to solvent-free TFI-IL-QDs (Fig. 5a). Additionally, a 3 wt% TFI-IL-QD solution displayed high dispersion stability without any NP aggregation for long-term storage (>2 months). As shown in Fig. 5b, the increase of TFI-IL-QD concentration enhanced the adsorbed amount of TFI-IL-QD onto the anionic PSS layer, thereby leading to typical adsorption isotherm behavior as confirmed by quartz crystal microgravimetry (QCM). The deposition time of TFI-IL-QDs with green emission onto QCM electrode was saturated within 10 min. For the 3 wt% TFI-IL-QD/PSS multilayers, the average mass change per layer adsorbed from the TFI-IL-QDs was approximately  $2.803 \pm 0.175 \mu\text{g cm}^{-2}$  (Fig. 5c). Film thickness was measured to be  $\sim 50$  nm. In this case, the TFI-IL-QDs solution was LbL-assembled with PSS without the addition of ionic salts or pH control. Considering that TFI-IL-QD<sub>green</sub> (*i.e.*, green emissive QDs) were composed of a 4 nm CdSe core with a density of  $5.81 \text{ g cm}^{-3}$  and a 1 nm thick ZnS shell with a density

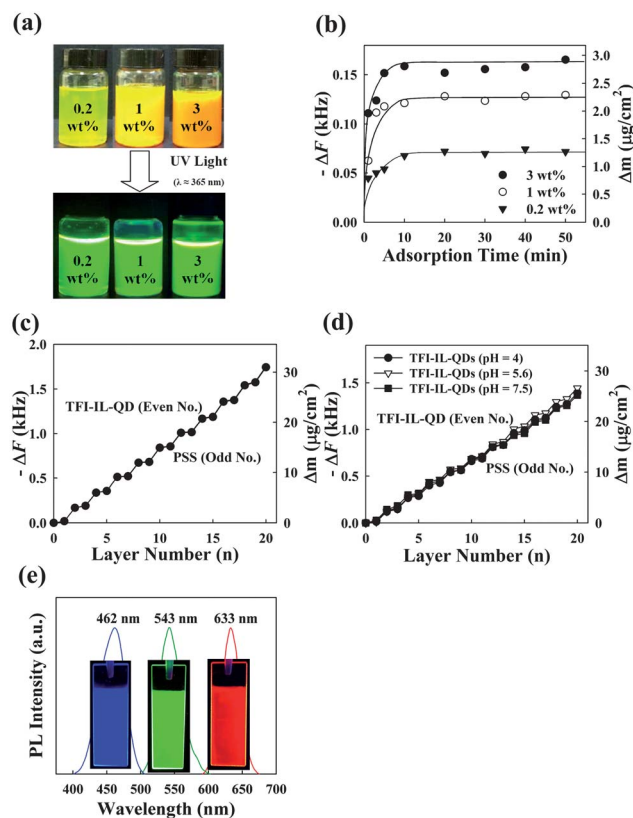


**Fig. 5** (a) Photo images of the positively charged TFI-IL-QD solution prepared for each concentration by adding water. (b) Adsorption isotherm behavior for positively charged TFI-IL-QD deposited onto QCM electrodes as functions of adsorption time and concentration. (c) Investigation of frequency and mass changes for (PSS/3 wt% TFI-IL-QD)<sub>n</sub> multilayers as a function of bilayer number by QCM measurement. (d) The adsorption amount of TFI-IL-QDs (1 wt%) as a function of pH by QCM measurement. (e) The PL spectra of (PSS/each-colored TFI-IL-QD)<sub>10</sub> multilayers. The photographic images in (e) show each-colored multilayers.

of  $3.89 \text{ g cm}^{-3}$ , the surface coverage of the TFI-IL-QD<sub>green</sub> per layer was approximately 45%, corresponding to a density of approximately  $1.0 \times 10^{12} \text{ cm}^{-2}$ . It is expected that this packing density will be further enhanced with increasing TFI-IL-QD concentration. These results are noticeable in that electrostatic repulsion between NPs of the same charge usually results in a low packing density for each component layer even at high concentration if there is no appropriate pH or ionic strength control over NP deposition solution.<sup>39,40</sup> Densely adsorbed TFI-IL-QDs are derived from the distribution of positive charges over the imidazolium ring's resonance structures despite strong electrolytes.<sup>41,42</sup> The adsorbed amount of TFI-IL-QD was negligibly influenced by solution pH (e.g., pH 4.0, 5.6, and 7.5), which was opposed to the strong pH-dependent adsorption behavior shown in weak electrolytes (Fig. 5d). The distribution of cationic states between two different nitrogen atoms within the imidazolium ring can decrease the electrostatic repulsion between adjacent TFI-IL-QDs without additional ionic salts. In contrast, quaternized ammonium-based materials, such as poly-(diallyldimethylammonium chloride), do not distribute charge through a resonance structure. Therefore, they require the addition of ionic salts to reduce the electrostatic repulsion between identically charged components for the formation of densely adsorbed layers onto oppositely charged materials.<sup>43</sup> For example, in the case of TFI-IL-QD/PSS, cysteamine (CA)-QDs/PSS, and mercaptoacetic acid (MA)-QD/poly(allylamine hydrochloride) (PAH) multilayer films prepared from the same QD concentration (i.e., 3 wt%) and solution pH (i.e., pH  $\approx$  5.6), the adsorbed amount of TFI-IL-QDs was higher than that of CA-QDs or MA-QDs (ESI, Fig. S7†). It should also be noted that the relative quantum yield ( $\sim$ 20.4%) of TFI-IL-QD<sub>green</sub> relative to coumarin 545 was higher than that of MA acid ( $\sim$ 9%) or CA-stabilized QD<sub>green</sub> ( $\sim$ 3.6%). Recent studies have also shown that a high packing density of smaller thiol ligands, such as MA acid or CA rather than TFI-IL, significantly reduces the QD quantum yield.<sup>44,45</sup> Therefore, (TFI-IL-QDs/PSS)<sub>10</sub> multilayers with red, green, and blue emissions showed a strong PL intensity due to relatively high quantum yield as well as a densely adsorbed amount (Fig. 5e); furthermore, these films emitted sufficiently intense white levels that were detectable by the naked eye through the overlap of blue-, green- and red-emissive multilayers (see ESI, Fig. S8†).

## Conclusions

We have demonstrated here for the first time that solvent-free metal NPs and QDs with notable electrical or optical properties can be prepared using the successive phase transfer from a nonpolar solvent medium to a thiol-containing imidazolium-type IL with a short chain length. Furthermore, these solvent-free NPs could be used to prepare the functional LbL multilayers with densely adsorbed NPs, allowing the facile control of NP concentration. The present strategy shown in our study could also be extended to a variety of solvent-free NP fluids with size-selective nanowires as well as spherical shapes due to their high affinity with the thiol group of TFI-IL. Therefore, we believe that our approach can be effectively applied to a variety of optical inks, printable electrodes for electronic devices, and active films for functional film devices.

## Acknowledgements

This work was supported by the National Research Foundation (NRF) grant funded by the Korea government (MEST) (2010-0029106 and 2010-0027751) and ERC Program of NRF grant funded by the Korea government (MEST) (R11-2005-048-00000-0).

## Notes and references

- 1 A. B. Bourlinos, R. Herrera, N. Chalkias, D. D. Jiang, Q. Zhang, L. A. Archer and E. P. Giannelis, *Adv. Mater.*, 2005, **17**, 234–237.
- 2 L. Sun, J. Fang, J. C. Reed, L. Estevez, A. C. Bartnik, B.-R. Hyun, F. W. Wise, G. G. Malliaras and E. P. Giannelis, *Small*, 2010, **6**, 638–641.
- 3 S. C. Warren, M. J. Banholzer, L. S. Slaughter, E. P. Giannelis, F. J. DiSalvo and U. B. Wiesner, *J. Am. Chem. Soc.*, 2006, **128**, 12074–12075.
- 4 J. Zhou, D. Tian and H. Li, *J. Mater. Chem.*, 2011, **21**, 8521–8523.
- 5 N. V. Plechkova and K. R. Seddon, *Chem. Soc. Rev.*, 2008, **37**, 123–150.
- 6 S. S. Moganty, N. Jayaprakash, J. L. Nugent, J. Shen and L. A. Archer, *Angew. Chem., Int. Ed.*, 2010, **49**, 9158–9161.
- 7 Z. Ma, J. Yu and S. Dai, *Adv. Mater.*, 2010, **22**, 261–285.
- 8 J. Dupont and J. D. Scholten, *Chem. Soc. Rev.*, 2010, **39**, 1780–1804.
- 9 A. Zabet-Khosousi and A.-A. Dhirani, *Chem. Rev.*, 2008, **108**, 4072–4124.
- 10 B. Y. Ahn, E. B. Duoss, M. J. Motala, X. Guo, S.-I. Park, Y. Xiong, J. Yoon, R. G. Nuzzo, J. A. Rogers and J. A. Lewis, *Science*, 2009, **323**, 1590–1593.
- 11 Z. Feng and F. Yan, *Surf. Interface Anal.*, 2008, **40**, 1523–1528.
- 12 H. Goesmann and C. Feldmann, *Angew. Chem., Int. Ed.*, 2010, **49**, 1362–1395.
- 13 L. Piao, K. H. Lee, W. J. Kwon, S.-H. Kim and S. Yoon, *J. Colloid Interface Sci.*, 2009, **334**, 208–211.
- 14 H. Bönemann, W. Brijoux, R. Brinkmann, E. Dinjus, T. Joußen and B. Korall, *Angew. Chem., Int. Ed. Engl.*, 1991, **30**, 1312–1314.
- 15 W. K. Bae, K. Char, H. Hur and S. Lee, *Chem. Mater.*, 2008, **20**, 531–539.
- 16 G. Decher, *Science*, 1997, **277**, 1232–1237.
- 17 F. Caruso, R. A. Caruso and H. Möhwald, *Science*, 1998, **282**, 1111–1114.
- 18 J. Choi and M. F. Rubner, *Macromolecules*, 2005, **38**, 116–124.
- 19 K. C. Krogman, J. L. Lowery, N. S. Zacharia, G. C. Rutledge and P. T. Hammond, *Nat. Mater.*, 2009, **8**, 512–518.
- 20 S. W. Lee, J. Kim, S. Chen, P. T. Hammond and S.-H. Yang, *ACS Nano*, 2010, **4**, 3889–3896.
- 21 P. Podsiadlo, A. K. Kaushik, E. M. Arruda, A. M. Waas, B. S. Shim, J. Xu, H. Nandivada, B. G. Pumplun, J. Lahann, A. Ramamoorthy and N. A. Kotov, *Science*, 2007, **318**, 80–83.
- 22 Y. Ko, Y. Kim, H. Baek and J. Cho, *ACS Nano*, 2011, **5**, 9918–9926.
- 23 B. Lee, Y. Kim, S. Lee, Y. S. Kim, D. Wang and J. Cho, *Angew. Chem., Int. Ed.*, 2010, **49**, 359–363.
- 24 M. Yoon, Y. Kim and J. Cho, *ACS Nano*, 2011, **5**, 5417–5426.
- 25 Y. Kim, C. Lee, I. Shim, D. Wang and J. Cho, *Adv. Mater.*, 2010, **22**, 5140–5144.
- 26 M. I. Dafinone, G. Feng, T. Brugarolas, K. E. Tettey and D. Lee, *ACS Nano*, 2011, **5**, 5078–5087.
- 27 D. Buttry, *Advances in Electroanalytical Chemistry: Applications of the QCM to Electrochemistry*, Marcel Dekker, New York, 1991.
- 28 A. G. Hemmersam, K. Rechendorff, F. Besenbacher, B. Kasemo and D. S. Sutherland, *J. Phys. Chem. C*, 2008, **112**, 4180–4186.
- 29 D. Thid, J. J. Benkoski, S. Svedhem, B. Kasemo and J. Gold, *Langmuir*, 2007, **23**, 5878–5881.
- 30 F. Höök, A. Ray, B. Nordén and B. Kasemo, *Langmuir*, 2001, **17**, 8305–8312.
- 31 G. Baleizao, B. Gante, H. Garcia and A. Corma, *Tetrahedron Lett.*, 2003, **44**, 6813–6816.
- 32 H. Yang, C. Shan, F. Li, D. Han, Q. Zhang and L. Niu, *Chem. Commun.*, 2009, 3880–3882.
- 33 Q. Li, L. Dong, J. Fang and C. Xiong, *ACS Nano*, 2010, **4**, 5797–5806.
- 34 Y. H. Hyun, S. T. Lim, H. J. Choi and M. S. Jhon, *Macromolecules*, 2001, **34**, 8084–8093.

- 35 D. Untereker, S. Lyu, J. Schley, G. Martinez and L. Lohstreter, *ACS Appl. Mater. Interfaces*, 2009, **1**, 97–101.
- 36 J. Zhu, S. Wei, Y. Li, L. Sun, N. Haldolaarachchige, D. P. Young, C. Southworth, A. Khasanov, Z. Luo and Z. Guo, *Macromolecules*, 2011, **44**, 4382–4391.
- 37 K. C. Beverly, J. F. Sampaio and J. R. Heath, *J. Phys. Chem. B*, 2002, **106**, 2131–2135.
- 38 R. Koole, P. Liljeroth, C. M. Donega, D. Vanmaekelbergh and A. Meijerink, *J. Am. Chem. Soc.*, 2006, **128**, 10436–10441.
- 39 M. Raposo and O. N. Oliveira, *Langmuir*, 2002, **18**, 6866–6874.
- 40 H. Jin, J. Nam, J. Park, S. Jung, K. Im, J. Hur, J.-J. Park, J.-M. Kim and S. Kim, *Chem. Commun.*, 2011, **47**, 1758–1760.
- 41 M. H. Allen, M. D. Green, H. K. Getaneh, K. M. Miller and T. E. Long, *Biomacromolecules*, 2011, **12**, 2243–2250.
- 42 D. X'iao, J. R. Rajian, A. Cady, S. Li, R. A. Bartsch and E. L. Quitevis, *J. Phys. Chem. B*, 2007, **111**, 4669–4677.
- 43 K. Glinel, A. Moussa, A. M. Jonas and A. Laschewsky, *Langmuir*, 2002, **18**, 1408–1412.
- 44 I. L. Medintz, H. T. Uyeda, E. R. Goldman and H. Mattoussi, *Nat. Mater.*, 2005, **4**, 435–446.
- 45 H. Mattoussi, J. M. Mauro, E. R. Goldman, G. P. Anderson, V. C. Sundar, F. V. Mikulec and M. G. Bawendi, *J. Am. Chem. Soc.*, 2000, **122**, 12142–12150.